Journal of Residuals Science & Technology (JRST) Volume 14 No. 3, 2017
doi: 10.14355/jrst.2017.1403.002

Synthesis, Characterization and Photocatalytic Performance of Lanthanides (Y, Ce) Doped TiO_2 Nanosheets Films

Yu Fu[a,b], Yufeng Wu[a,b,*], Qijun Zhang[a,b], Kaihua Zhang[a,b], Xiaofei Yin[a,b], Yi-Nan Zhang[c]

[a] Institute of Circular Economy, Beijing University of Technology, Beijing, 100124, P. R. China.

[b] Institute of Beijing-Tianjin-Hebei Green Development, Beijing University of Technology, Beijing, 100124, P. R. China.

[c] Institute of Biomaterials and Biomedical Engineering, University of Toronto, Toronto, ON M5S 3G9, Canada.

*Corresponding Author: Fax: +86-10-67396234; Tel: +86-10-67396234;

*wuyufeng3r@126.com

Abstract

Different lanthanides (Y, Ce) ions doped anatase TiO_2 nanosheets films with dominant high-reactivity {001} facets were synthesized on transparent conductive FTO substrates via a simple, one-step solvothermal method. In the present work, the amounts of HF and the doping ratios of rare earths were explored in detail. The crystal morphologies, structural features, binding information, optical absorption, and photocatalytic performances were investigated systematically. The optimal conditions of HF amount and rare earths doping ratios proved to be 2 mL and 1.0%, respectively. The results showed that the optimum lanthanides (Y, Ce) doped anatase TiO_2 nanosheets films displayed higher photocatalytic activities than pure TiO_2 films, and Y doped TiO_2 showed better photocatalytic activity than Ce doped TiO_2. The possible mechanism of the photocatalysis can be mainly ascribed to the synergistic effect of lanthanides doping and exposed high-reactively {001} facets.

Keywords

TiO_2; Nanosheets; Lanthanides Doped; {001} Facets; Photocatalytic Activities

Introduction

As a sustainable technology, nanostructure TiO_2-based photocatalysis has received much attention in the last few decades because it has potential to use in the fields of energy and the environment, such as dye-sensitized solar cells [1-5], hydrogen production [6, 7] and photocatalytic degradation [8-11], etc. However, some weaknesses still exist in practical utilization of nanostructure TiO_2 photocatalyst. TiO_2 has a wide band gap of 3.24 eV [12-14], which leads to a low utilization ratio of solar energy. On the other hand, high recombination of electron-hole pairs decreases the photo-quantum efficiency.

To solve these problems, a great number of studies have focused on how to modify TiO_2 doped with ions such as noble metals [15, 16], nonmetals [17-19], rare earths (RE) elements [20-22], etc. Among these, the modifying by RE elements has turned out to be a feasible and promising strategy due to the 4f electron configuration of RE elements, which can reduce the electron-hole pair recombination [23-27]. Moreover, the modification by RE elements can increase the photoadsorption of organic substrates on the TiO_2 surfaces, which also enhances the photocatalytic performance. For example, Duan *et al*. [28] prepared praseodymium doped TiO_2 (Pr-TiO_2), which showed that the

redox activity was influenced by the position of the band edge and the photocatalytic performance was improved by introducing doping rare earth. Meski *et al.* [25] prepared lanthanum doped TiO_2 (La-TiO_2). The photocatalytic performance of TiO_2 was improved because La shortened the bandwidth of TiO_2 and decreased the recombination rate of photo-generated electron-hole pairs.

According to density functional theory [12, 29], the common surface energies of certain anatase facets are 0.9 J/m^2 of {001}, 0.53 J/m^2 of {100}, 0.44 J/m^2 of {101} [30, 31]. Although the theory cannot represent the actuality, the result is still meaningful: {001} facets show a higher reactive activity than {101} facets, and the anatase TiO_2 is commonly formed by (101) facets with stable thermodynamic properties due to its low surface energy [32-34]. Since theresearch by Yang *et al.* [35] in 2008 who successfully synthesized TiO_2 with 47% exposed {001} facets, many researchers have been exploring the properties and performances of the {001} facets as well as how to prepare TiO_2 with high percentage of exposed {001} facets.

The advantages of rare earth doping and the {001} facets controlling are obvious. However, few studies have been focused on the synergistic effects of both lanthanides ions doped TiO_2 nanosheets and the morphological control of expose {001} facets, which may contribute to excellent photocatalytic activity. Here, we investigate the synthesis of lanthanides (Y, Ce)-doped anatase TiO_2 nanosheets films with dominant high-reactivity {001} facets on fluorine-doped tin dioxide (FTO), which was proved to be of better stability than Indium tin oxide (ITO) and common glass in HF [36]. In addition, the effects of different doping amounts of REs on the characteristics of TiO_2 such as the morphologies, structures, luminescence properties, and the photocatalytic performances are studied systematically.

Experiment Section

Chemicals and Materials

All reagents used in this study were of the highest available purity, purchased from Chemical Reagent Company of Beijing. Deionized water (18.2 MΩ.cm) obtained from a Direct-Pure Up 10 water system (RephiLe Bioscience, Ltd.) was used through the experiments whenever needed. The FTO substrates used in this study were purchased from Shenzhen CSG Float Glass Co. Ltd (Shenzhen, China).

Synthesis

A solvothermal method is used to prepare lanthanides (Y, Ce) doped TiO_2 nanosheets films on FTO substrates. The FTO substrates are prepared with sizes of 2.0 × 4.0 cm^2, and cleaned ultrasonically by deionized water, acetone, and ethanol for 1 h separately. In most experiments, 40 mL of acetic acid (HAc) is mixed with rare earth nitrate ($RE(NO_3)_3$), 10 mL of tetrabutyl titanate ($Ti(OBu)_4$), and appropriate amount of hydrogen fluoride (HF). Every chemical is added with uniform stirring. First, a proper amount of HF are considered to explore the impact of photocatalytic properties. Then, the molar ratios of RE elements and Ti are investigated in the range of 0.25%, 0.5%, 1.0%, 1.5%, and 2.0%, respectively. The solution is transferred into a 100 mL Teflon-lined autoclave, and the FTO substrate is on the bottom of the autoclave with the conductive surface facing upward. The solution is kept at 200 °C for 12 h. Having finished the reaction, the FTO substrates with RE-TiO_2 films are pick out and washed with ethanol several times, then dried at 60 °C for 24 h. Finally, all the RE-TiO_2 films are calcined at 500 °C for 6 h with a rate of 1 °C/min.

Characterization

The crystal structure is examined by X-ray diffraction (XRD) analysis with a Bruker axs D8 Advance using Cu Kα

radiation (Bruker, Germany). The morphology of the samples is examined by JEM-2100F high-resolution transmission electron microscopy (TEM) (JEOL, Japan) and SU-8020 field-emission scanning electron microscopy (SEM) (Hitachi, Japan). The diffuse reflectance spectra (DRS) are characterized by an UV-vis spectrophotometer (UV 2550, Shimadzu, Japan). X-ray photoelectron spectroscopy (XPS) data are obtained with an ESCALab220i-XL electron spectrometer from VG Scientific using 300 W Al KR radiation (E = 1486.6 eV) in a base pressure of 3×10^{-9} m bar. The binding energies are referenced to the C 1s line at 284.8 eV from adventitious carbon. The photoluminescence (PL) spectra are tested with a Japan Hitachi F7000 fluorescence spectrophotometer using a 330 nm line from a xenon lamp.

Evaluation of Photocatalytic Properties

The photocatalytic properties of the samples are compared by analyzing the degradation rates of Methylene Blue (MB) and Methyl Orange (MO). All of the RE-TiO_2 films of 2.0 cm × 4.0 cm are used. Before being tested, all of the samples are immersed in a sodium hydroxide (NaOH) solution (5 mol/L, 50 mL) for 1 h, washed with deionized water several times, and then dried. To establish the adsorption-desorption equilibrium, samples are submerged in organic solution (MB/MO, 10 mL, 10 mg/L) in 60 mm culture dishes separately for 12 h. In the experiment, a 30 W UV lamp with a maximum emission at approximately 365 nm was used as the illumination source. And the absorption of organic solutions (MB/MO, 10 mL, 10 mg/L) are measured every 1 h by the ultraviolet spectrophotometer. The data are analyzed by recording the absorption peaks of MB at 664 nm and MO at 465 nm.

Results and Discussion

HF, with the strong corrosion ability, is usually employed as capping agent in experiments. Our initial research focused on identifying a proper amount of HF to obtain TiO_2 with high active reactive {001} facets. Here, pure TiO_2 is used to study the impact of HF on the {001} faces by regulating the addition of HF amounts in the range of 0 mL, 1 mL, 2 mL and 3 mL. Figure 1 shows the SEM images in different HF amounts, and the simulated shapes are showed in Figure SI-1 [30, 37]. As can be seen in Figure 1(a), the nanoparticles show an integral bipyramidal structure, and the isosceles triangular sidewalls are the {101} facets. In Figure 1(b), the bipyramid are partly eroded. The isosceles trapezoidal sidewalls are the {101} facets, and the flat squares are the {001} facets. In Figure 1(c), the nanoparticles are further eroded into flakes. As is shown in Figure 1(d), there are some nanopores in every flake. The erosion of TiO_2 nanosheets are increased with the increase of HF concentration. Definitely, HF can selectively erode {001} facets because titanium and oxygen on the surface of the {001} and {101} facets have different geometric arrangement. At high concentration, HF selectively etches {001} facets by the -OH replacement and -$TiOF_2$ dissolution on the surface of {001} facets [38]. According to the above results, the samples have the highest percentage of exposed {001} facets at 2 mL of the HF addition. As a result, 2 mL of HF is used for all subsequent experiments.

The crystalline phases of synthesized pure and doped TiO_2 are examined by XRD. As shown in Figure 2, the intensity peaks of all samples are consistent with the crystal structure of tetragonal-anatase TiO_2 with $I4_1/amd$ space group symmetry (JCPDS No. 21-1272) [39, 40], indicating that the high crystallinity of these products [41] (Figure 2a). However, we notice that no other crystalline phases (such as Y_2O_3, Ce_2O_3 or CeO_2) are observed, which suggest that rare earth ions might be well dispersed on the surface of TiO_2. It can be observed that the main diffraction peaks (101) have a negligible shift to high degrees after rare earth ions doping compared with pure TiO_2 nanosheets, as shows local amplification (Figure 2(b)). It is suggested that there are small contortions in the TiO_2 lattices [42]. Actually, the ionic radii of rare earth elements are much larger than Ti^{4+} (Y^{3+}, Ce^{3+}, Ce^{4+} and Ti^{4+} are

101.9 pm [43], 98 pm, 114 pm [44] and 60.5 pm [43], respectively), which make it difficult for rare earth ions to enter into the TiO_2 lattice. Thus, the small contortions in the TiO_2 lattices may due that some rare earth ions present on the grain boundaries [45] or replace Ti^{4+} on the surface.

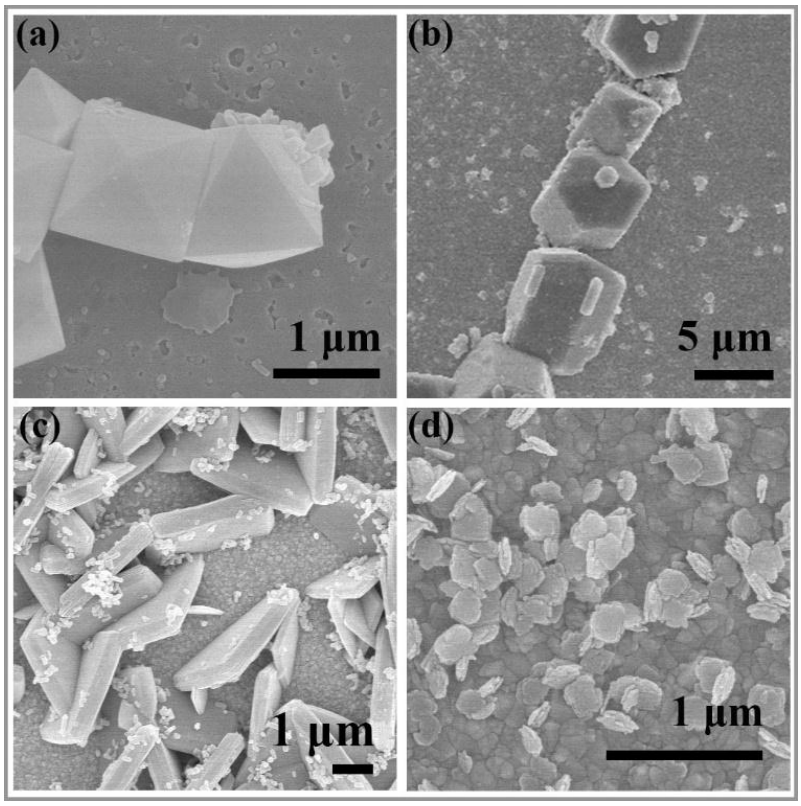

FIG. 1 SEM PATTERNS OF PURE TIO_2 FILMS USING (A) 0 ML, (B) 1 ML, (C) 2 ML AND (D) 3 ML HF CONTENTS

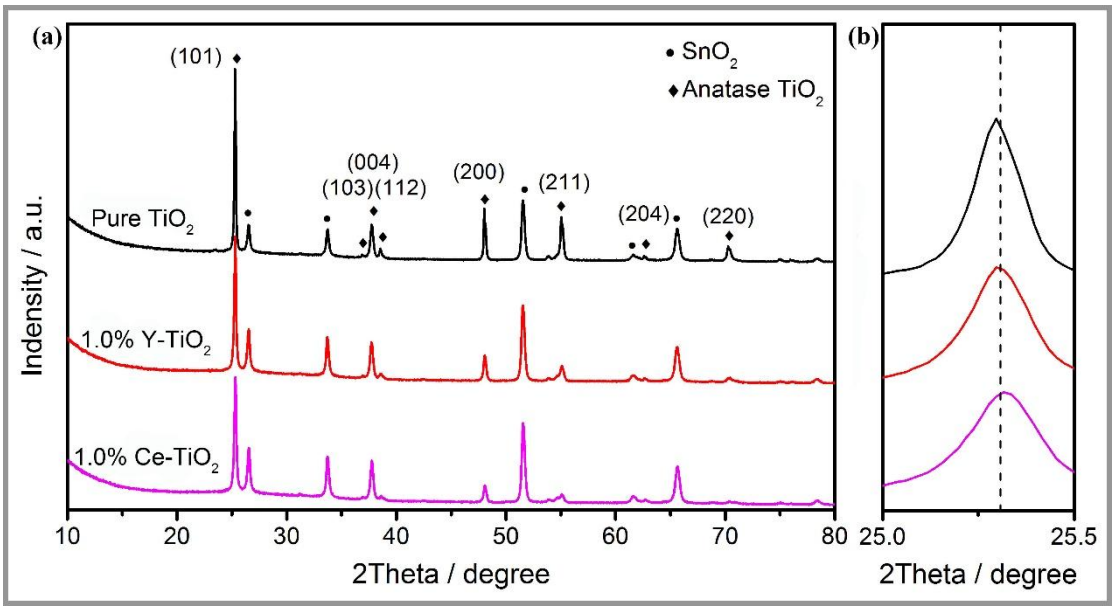

FIG. 2 XRD PATTERNS OF THE PURE TIO_2 AND 1.0% RE-TIO_2. (A) INTEGRAL XRD PATTERN AND (B) SECTIONAL XRD PATTERNS

TEM is employed to characterize the crystallographic structures of the RE-TiO_2 nanosheets and pure TiO_2 nanosheets samples, as shown in Figure 3. Figure 3(a-c) shows that all the pure and doped TiO_2 samples have uniform layer-structured sheets structures. The high-resolution TEM image of the sheet structure lying on the TEM

grid suggest that the lattice spacing parallel was 0.19 nm, in good agreement with the spacing of the (200) and (020) lattice planes of the TiO_2 (Figure 3(g)) [46]. The diffraction spots in selected area electron diffraction (SAED) patterns (Figure 3(d)) are measured, resulting in corresponding to the facets of (200) and (020) facets, which means that the top and bottom facets observed are both {001} facets. The HRTEM images of RE-TiO_2 nanosheets (Figure 3(h-i)) directly reveal that the lattice spacing parallel is 0.235 nm, indicating that the top and bottom facets of the RE-TiO_2 nanosheets are the {001} facets [47]. Moreover, the corresponding SAED pattern (Figure 3(e-f)) can be indexed into the diffraction spots of the [001] zone, which also confirm that the faceted surface of RE-TiO_2 nanosheets is the (001) surface.

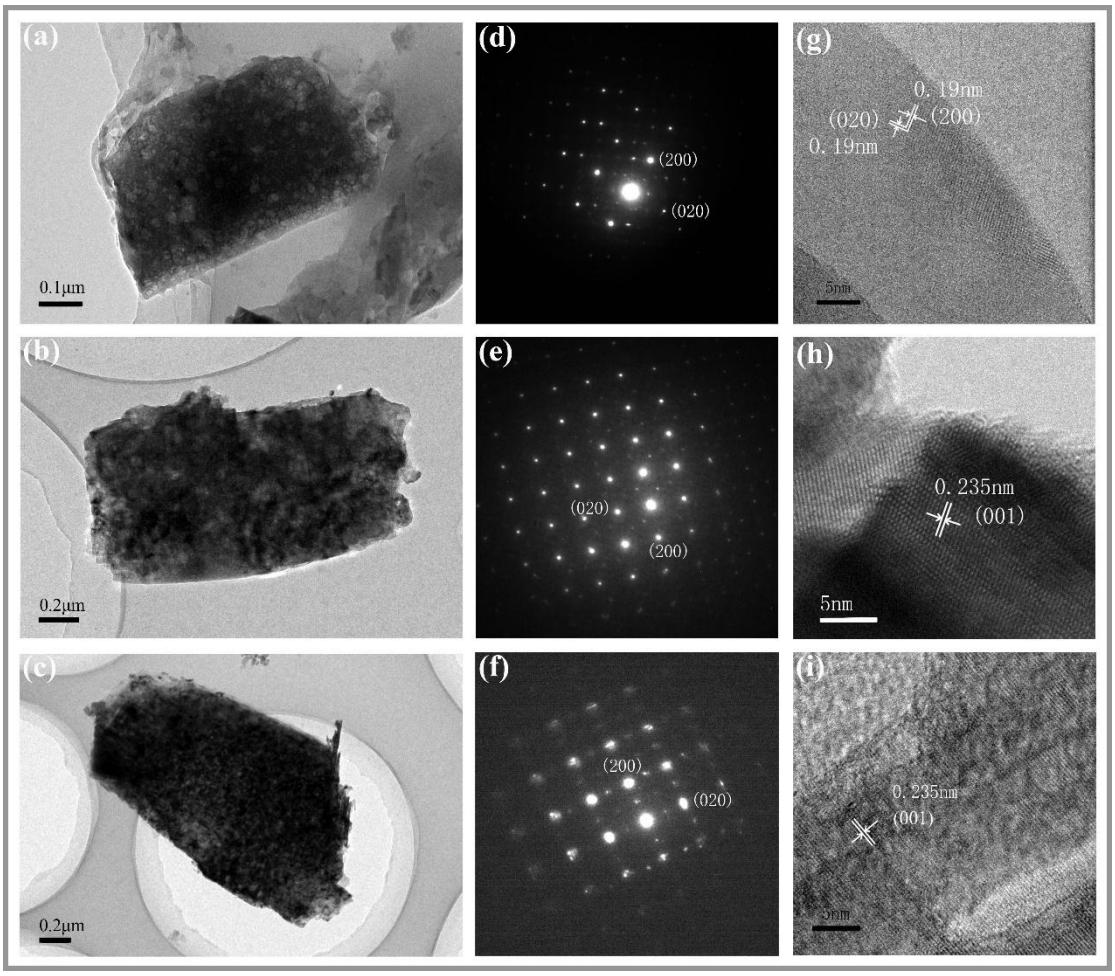

FIG. 3 TEM PATTERNS OF (A, D, G) PURE TIO_2, AND (B, E, H) 1.0% Y-TIO_2, AND (C, F, I) 1.0% CE-TIO_2. (A-C) ARE TEM PATTERNS, (D-F) ARE SAED PATTERNS, (G-I) ARE HRTEM PATTERNS

Figure 4 shows SEM images of pure and doped TiO_2 nanosheets samples. As illustrated, all of pure and doped TiO_2 nanosheets samples show well-defined nanosheets morphological structures with two exposed {001} facets in agreement with TEM results and the growth of most nanosheets are perpendicular to the substrate. The typical crystal type of TiO_2 belongs to the tetragonal system. The thickness of RE-TiO_2 is in the range of 0.14 - 0.4 μm, the sample length is 1.7 - 3.5 μm, and the length on the plane of fracture is 0.9 - 2.8 μm. However, the thickness of pure TiO_2 is 0.6 μm. Obviously, doping with rare earth elements cannot change the crystal structures according to the XRD results, but can decrease the thickness of TiO_2. The relative sizes of as-prepared TiO_2 are measured according to the SEM images, as shown in Table SI-1. The percentage of the {001} facets is calculated by the measured sizes (shown in Figure SI-1(d)). As is shown in Table 1, the percentage of the {001} facets exceed 80% at 1.0% RE-TiO_2,

among which the percentages of the {001} facets at 1.0% Y-TiO_2 and 1.0% Ce-TiO_2 are 91% and 92%, respectively. It can be seen that the percentage of the {001} facets has a trend of increasing with the adding of RE nitrates because RE ions can accelerate the anisotropic platelet growths of TiO_2 crystallites [13]. However, the percentage of {001} facets decreases at higher doping levels in the range of 1.0-2.0%, which can be ascribed to the introduction of too much nitrate ions (NO_3^-). It has been reported that nitrate ions (NO_3^-) can adsorb onto the surface of the nucleus and reduce the adsorption capacity of the fluoride ions, and thus decreasing the percentage of the {001} facets [48].

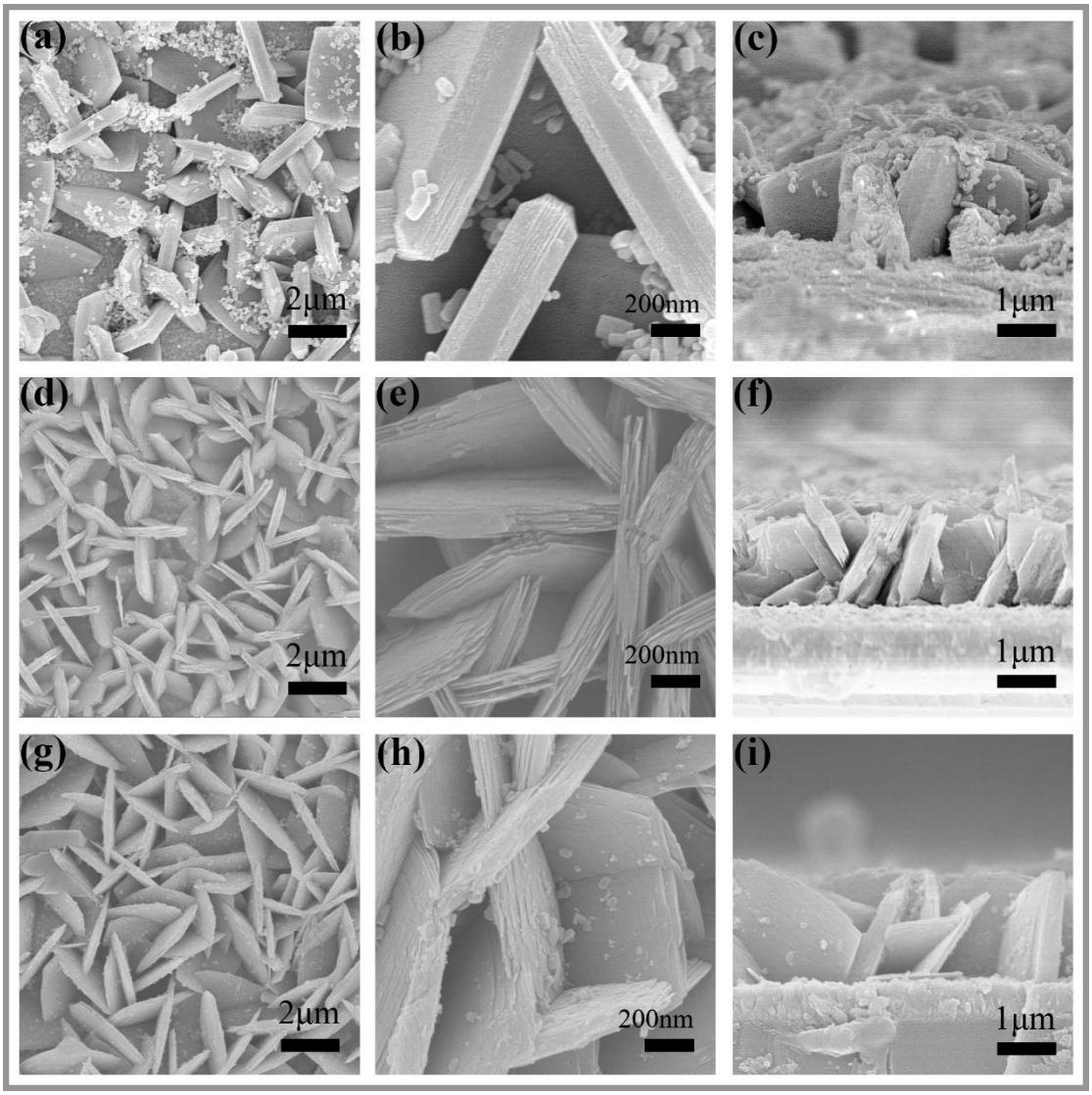

FIG. 4 SEM PATTERNS OF RE-TIO_2 FILMS. (A-C) PURE TIO_2 FILMS, (D-F) 1.0% Y-TIO_2 FILMS, (G-I) 1.0% CE-TIO_2 FILMS. AND (C-I) ARE CROSS-SECTIONAL SEM PATTERNS OF PURE TIO_2 FILMS AND 1.0% RE- TIO_2

TABLE 1 SUMMARY OF STRUCTURAL PARAMETERS OF SAMPLES

Samples	Average Thickness (μm)	Average lateral length (μm)	Average height (μm)	Percentage of {001} facets (%)
TiO_2	0.6	3.2	1.8	66
1.0% Y-TiO_2	0.15	3.5	2.5	91
1.0% Ce-TiO_2	0.25	3.2	1.9	92

Doping has a significant effect on adjusting the number of active group and combination ratios of electron-hole pairs. To confirm the element compounds and the valence states of elements, the as-prepared anatase RE-TiO_2 nanosheets films were investigated by XPS (Figure 5). As shown in Figure 5(a), the Ti 2p peaks of pure TiO_2 are present at 458.8 eV (Ti $2p_{3/2}$) and 464.5 eV (Ti $2p_{1/2}$). The difference value of 5.7 eV between the two bands suggests that Ti exists in the Ti^{4+} state [49]. The peaks of two kinds of 1.0% RE-TiO_2 are all shifted to higher binding energy compared with pure TiO_2, which is likely due to the orbits hybridization of rare earth cations and O anion [50, 51]. Moreover, the increasing ionic banding energy results from charge transfer between occupied O 2p and empty RE 3d orbitals [52], which likely results in narrower banding gap. The O 1s spectrum is shown in Figure 5(b). The peak of pure TiO_2 at 529.7 eV matches with the lattice O atoms, and the peak at 531.7 eV matches with the surface hydroxide groups, nearly corresponding with the literature [24]. The hydroxyl groups can trap holes, which inhibits the combination of electron-hole pairs, resulting in the enhancement of photocatalytic performance. In Figure 5(c), the peaks at 159.9 eV and 158.1 eV correspond to Y $3d_{3/2}$ and Y $3d_{5/2}$, which means that Y exists as yttrium oxide (Y_2O_3), in agreement with the literature [21]. The combinations of Y and O can create more oxygen vacancies, which delay the combination of photo-generated electron–hole pairs. [53]. In Figure 5(d), four peaks are present in the Ce 3d spectrum, and two peaks (p1 and p3) are in agreement with the Ce $3d_{3/2}$ spin-orbit state. The two peaks (p2 and p4) are in agreement with the Ce $3d_{5/2}$ spin-orbit state, which means that Ce^{3+}/Ce^{4+} exist at the same time [54]. The existence of Ce^{3+} (p1 and p3) means that a portion of the Ce ions exists as cerium oxide (Ce_2O_3). The other Ce^{3+} ions are oxidized to become Ce^{4+}, which suggests that Ce ions can form more oxygen vacancies [27, 55]. In summary, the XPS spectrum illustrates that rare earth ions are definitely doped into the TiO_2.

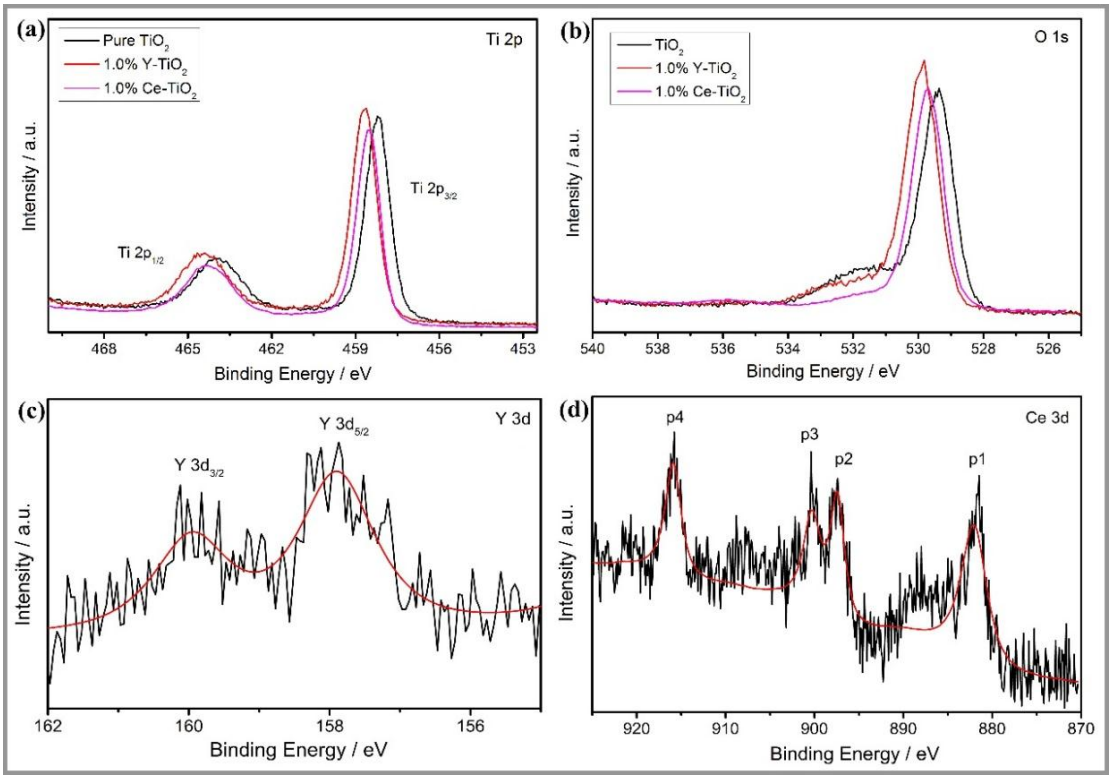

FIG. 5 XPS SPECTRA OF (A) PURE TiO_2 AND RE-TiO_2 SAMPLES FOR TI 2P, (B) PURE TiO_2 AND RE-TiO_2 SAMPLES FOR O 1S, (C) 1.0% Y-TiO_2 FOR Y 3D, (C) 1.0% CE-TiO_2 FOR 3D

The UV-vis DRS spectra plays a crucial role in detecting the optical properties and confirming whether the rare earth elements are doped in TiO_2. In Figure 6, the band gap of TiO_2 is 3.29 eV, which is close to the value of 3.24 eV in the literature [56]. The band gaps of RE-TiO_2 samples are decreased, which means the absorption band is moved

to the visible region slightly. The red shift indicates that the doping of the rare earth ions can expand the response range of the spectrum to the visible region. Figure 6(b) is the local amplification of a region in Figure 6(a). The different band gaps in Figure 6(b) illustrates that Y-TiO_2 (3.17 eV) has a narrower band gap than Ce-TiO_2 (3.25 eV), resulting from different doping levels.

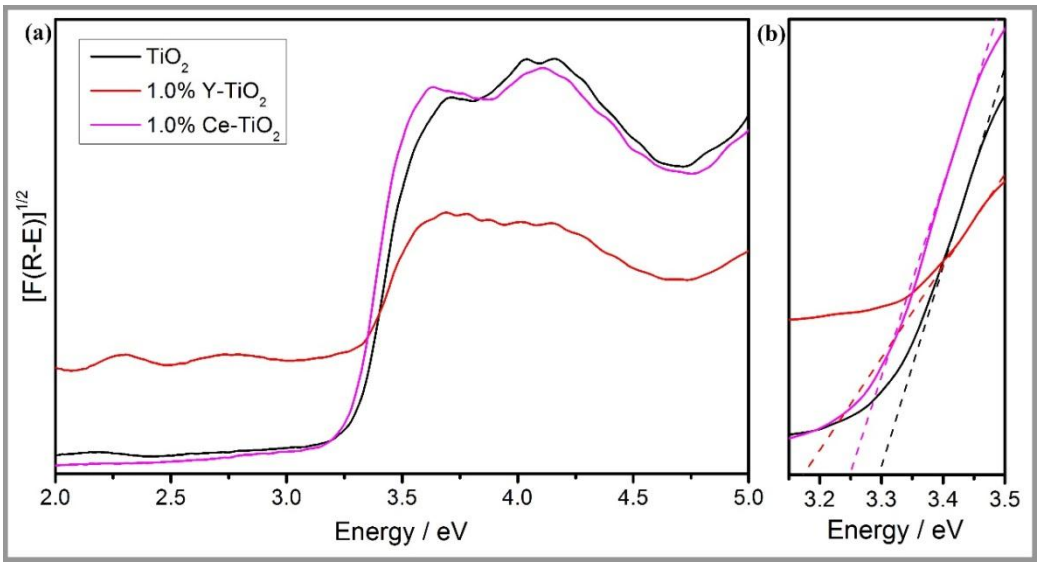

FIG. 6 UV-VIS DRS SPECTRA OF PURE TIO_2 FILMS AND 1.0% RE-TIO_2 FILMS. (A) INTEGRAL DRS SPECTRA AND (B) SECTIONAL DRS SPECTRA

It has been known that TiO_2 modification with lanthanides ions yield excellent electrons scavenging capacity and increase separation efficiency of electron-hole pairs [19]. Thus, we used the PL technique to measure the separation capacity of photo-generated electrons and holes of pure and RE-TiO_2 nanosheets films. Figure 7 shows the PL spectra of pure and RE- TiO_2 nanosheets films. Compared with the pure TiO_2, the RE- TiO_2 samples exhibit lower intensity of emission spectrum, which clearly indicates that a more efficient transfer and separation of electrons and holes caused by doped RE ions. However, the results also show that Y-doped TiO_2 has the lower intensity of emission spectrum than Ce-doped TiO_2.

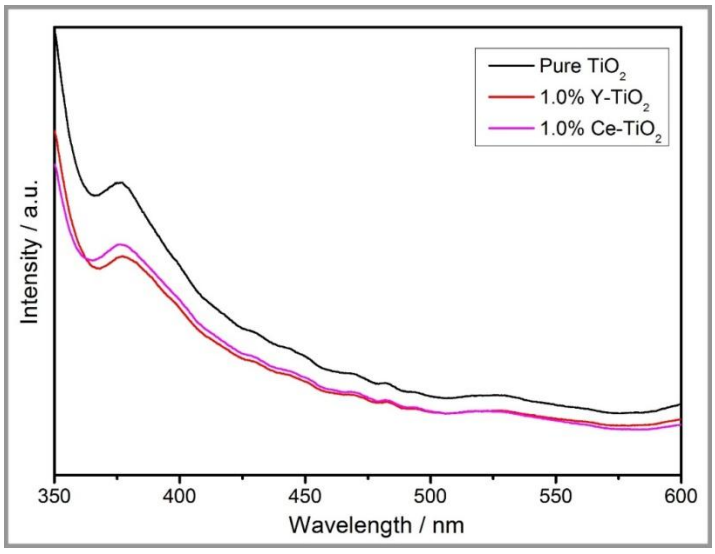

FIG. 7 PL SPECTRA OF PURE TIO_2 AND RE-TIO_2 SAMPLES

It is widely accepted that organic dyes can severely contaminate the environment. MB and MO are the representative of organic dyes. As a result, they are usually chosen as a metric for photocatalytic performance. Blank samples (organic solution without catalyst samples under irradiation) are also tested for comparison to avoid the influence of the dye sensitization. The degradation ratios equals to C_t/C_0 (C_0 and C_t represent the initial concentration of dyes and the concentration at time t). The reaction rate constant named symbol κ equals to $[\ln(C_t/C_0)]/t$ [57], which representing as the speed of degradation.

Figure 8a summarizes the photocatalytic performance of TiO_2 doped with 1.0% rare earth under UV light irradiation by degrading the MB solution. The degradation rate of the blank MB solution under UV light irradiation is approximately 30%. On the other hand, the photocatalytic activity is apparently improved when the Y-TiO_2 are dipped in MB solution. It is obvious that the photocatalytic performance of the TiO_2 films doped with rare earth has been improved compared to pure TiO_2 films. In Figure SI-2a, it is observed that the photocatalytic performance increases when the doping molar ratio is less than 1.0% and has a contrasting trend of decreasing from 1.0 - 2.0%. This means that the optimal doping amount is 1.0%, which is to say that the Y-TiO_2 films have higher photocatalytic performance than other molar ratios under 2.0%. When the molar ratio of Y/Ti reaches 1.0%, the degradation rate is highest in this experiment. Generally, the reaction rate of degrading organic dyes actually corresponds to photo-generated ·OH radicals decomposing organic dyes. The reaction rate constant is the highest in Y-TiO_2 films, as shown in Figure SI-2b, which approximately equals 7.01×10^{-3} min^{-1} (Table 2).

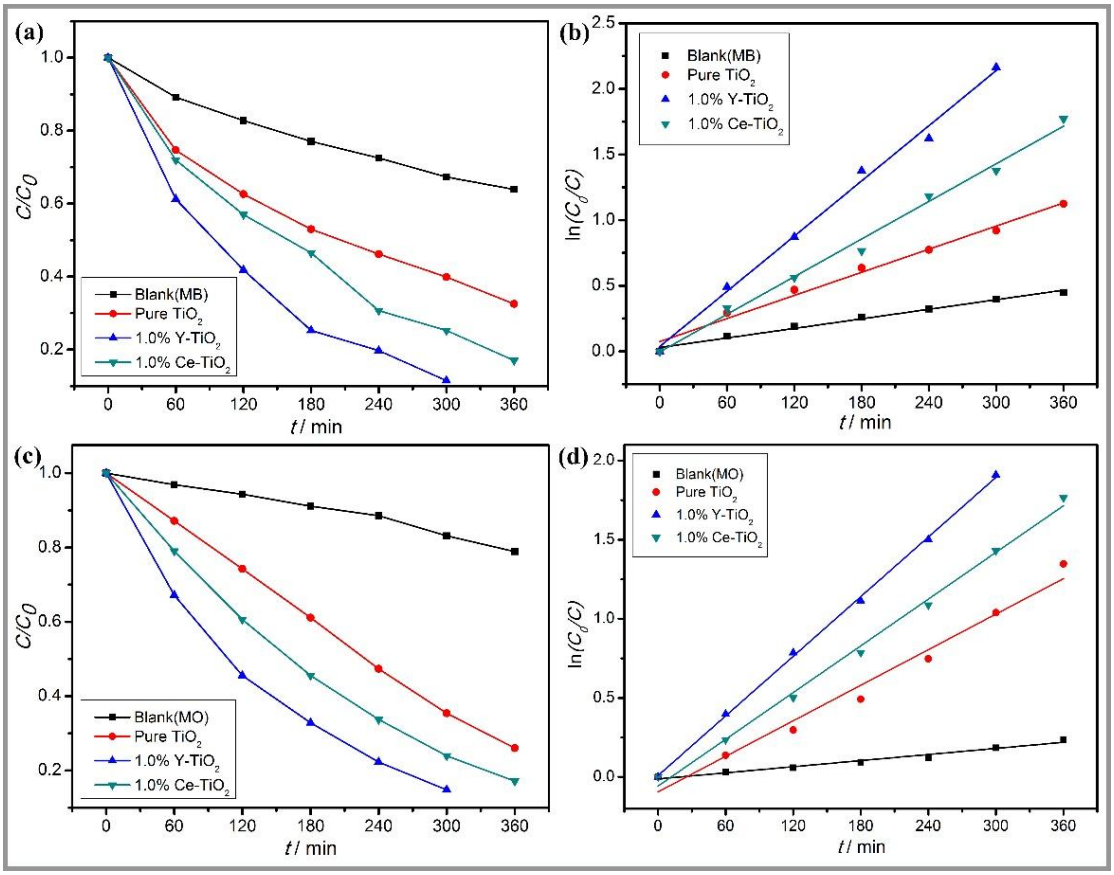

FIG. 8 (A) DEGRADATION RATIOS OF DIFFERENT SAMPLES FOR DEGRADING MB SOLUTIONS, (B) VARIATIONS IN $[\ln(C_T/C_0)]/T$ AS A FUNCTION OF IRRADIATION TIME AND LINEAR FITS OF DIFFERENT SAMPLES FOR DEGRADING MB SOLUTIONS, (C) DEGRADATION RATIOS OF DIFFERENT SAMPLES FOR DEGRADING MO SOLUTIONS, (D) VARIATIONS IN $\ln(C_T/C_0)$ AS A FUNCTION OF IRRADIATION TIME AND LINEAR FITS OF DIFFERENT SAMPLES FOR DEGRADING MO SOLUTION

TABLE 2. SUMMARY OF DEGRADATION RATES AND REACTION RATE CONSTANTS OF RE-TiO_2 SAMPLES FOR DEGRADING MB AND MO.

Samples	Degrading Ratios of MB (%) (after 5 h)	reaction rate constant of MB (min^{-1})	Degrading Ratios of MO (%) (after 5 h)	reaction rate constant of MO (min^{-1})
Blank	67.3	1.21×10^{-3}	83.1	0.64×10^{-3}
TiO_2	40.0	2.94×10^{-3}	35.4	3.75×10^{-3}
1.0% Y-TiO_2	11.5	7.01×10^{-3}	14.8	6.28×10^{-3}
1.0% Ce-TiO_2	25.2	4.78×10^{-3}	23.9	4.92×10^{-3}

To ensure the effect on the photocatalytic activity, an expanded experiment involving the degradation of MO solution is measured under UV light irradiation. The summary of the photocatalytic performance of the TiO_2 samples is shown in Figure 8c and Figure 8d. The reaction rate constant of pure TiO_2 and Y-TiO_2 (shown in Figure SI-2(c-d)). are 3.75×10^{-3} min^{-1} and 6.28×10^{-3} min^{-1}, which suggest that the reaction rate constant of Y-TiO_2 is about two times faster than the value for pure TiO_2 nanosheets samples. It is clear that superior photocatalytic performance is related to appropriate amounts of doping, low banding gap energy, a high percentage of exposed high-activity {001} facets, and a high density of nanosheets. The photocatalysis results show that TiO_2 nanosheets films doped with rare earth elements can optimize the photocatalytic activity compared to pure TiO_2 nanosheets films.

The photocatalytic activities of Ce-TiO_2 (Figure SI-3) have similar trends compared with Y-TiO_2. However, Y-TiO_2 have better photocatalytic performances than Ce-TiO_2, and RE-TiO_2 have better photocatalytic performances than pure TiO_2. In the degradation of MB and MO solution, the degradation rate of 1.0% Y-TiO_2 reaches 88.5% and 85.2% after 5 h, the degradation rate of 1.0% Ce-TiO_2 reaches 83.0% and 82.8% after 6 h as well, and both of them have surpassed the pure TiO_2 of 20%, the degradation rate of pure TiO_2 is only 60%.

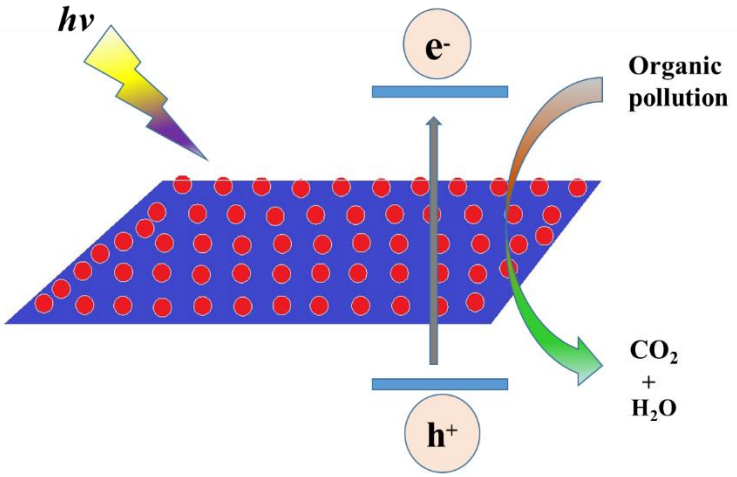

FIG. 9 PHOTOCATALYTIC PROCESSES ON RE-TiO_2 SURFACE UNDER UV-LIGHT IRRADIATION

Base on the photocatalytic experiment results, the enhanced photocatalytic activities of lanthanides (Y, Ce) doped anatase TiO_2 nanosheets films can be mainly resulted from the synergistic effects of lanthanides doping and exposed high-reactively {001} facets.(Figure 9) Lanthanides ions yield excellent electrons scavenging capacity and

increase separation efficiency of photo-generated electron-hole pairs. When lanthanides ions are doped onto the crystal surface or into lattices, the lattices are distorted and the charges lose balance [58]. To redress this imbalance, oxygen vacancies are formed in the vicinity, which can act as the active center of the reaction to inhibit the recombination of charge carriers. Therefore, these lanthanides (Y, Ce) ions, as impurities, form active trapping centers to trap photoelectron, which contributes to reactions with adsorbed O_2 and form highly reactive superoxide ions ($\cdot O_2^-$) [59]. Superoxide ions ($\cdot O_2^-$) can strongly reactive with organic molecules. Furthermore, doping with rare earth elements caused a red shift in photo-response, which can increase more photons were absorbed by samples. The results of the UV-vis DRS spectra confirmed that the band gaps of the doped TiO_2 samples are reduced.

Conclusion

Different lanthanides (Y, Ce) ions doped anatase TiO_2 nanosheets films with dominant high-reactivity {001} facets have been synthesized on FTO substrates via a simple, one-step solvothermal method. Compared to the pure TiO_2 films, Lanthanides (Y, Ce) ions doped TiO_2 nanosheets films showed better photocatalytic efficiency. The degradation rate of 1.0% RE-TiO_2 reaches over 80%, both of which have surpassed the pure TiO_2 of 20%. The as-prepared TiO_2 films reveal that different photocatalytic properties result from different concentration of solutions with different types of rare earth elements. 2 mL of HF and 1.0 mol% of RE-TiO_2 are the most appropriate amount.

RE-TiO_2 don't have any obvious differences in mechanism. Therefore, the results can be the theoretical support for the modified TiO_2 co-doped by yttrium and cerium, which can set as raw material to avoid further separation from primary ore or the original waste tricolor phosphors. We hope that this study would provide a new route for the modification of TiO_2 materials and offer methods for environmental management and energy proposal.

Acknowledgements

This research was financially supported by National Natural Scientific Foundation of China (No. 21306004), Beijing Nova Program (Z1511000003150141), Academician Workstation in Yunnan Province.

References

[1] Yahav, S., et al., Strong Efficiency Enhancement of Dye-Sensitized Solar Cells Using a La-Modified TiCl4 Treatment of Mesoporous TiO2 Electrodes. The Journal of Physical Chemistry C, 2011. 115(43): p. 21481-21486.

[2] Manca, M., et al., 3D Photoelectrode for Dye Solar Cells Realized by Laser Micromachining of Photosensitive Glass. The Journal of Physical Chemistry C, 2014. 118(30): p. 17100-17107.

[3] Roelofs, K.E., S.M. Herron and S.F. Bent, Increased Quantum Dot Loading by pH Control Reduces Interfacial Recombination in Quantum-Dot-Sensitized Solar Cells. ACS Nano, 2015. 9(8): p. 8321-8334.

[4] Wu, M. and T. Ma, Recent Progress of Counter Electrode Catalysts in Dye-Sensitized Solar Cells. The Journal of Physical Chemistry C, 2014. 118(30): p. 16727-16742.

[5] Punnoose, D., et al., Reduced recombination with an optimized barrier layer on TiO2 in PbS/CdS core shell quantum dot sensitized solar cells. New J. Chem., 2016. 40(4): p. 3423-3431.

[6] Li, S., et al., Photoelectrochemical Hydrogen Production of TiO2 Passivated Pt/Si-Nanowire Composite Photocathode. ACS Applied Materials & Interfaces, 2015. 7(33): p. 18560-18565.

[7] Xie, S., et al., Solid state precursor strategy for synthesizing hollow TiO2 boxes with a high percentage of reactive {001} facets exposed. Chemical Communications, 2011. 47(23): p. 6722-6724.

[8] Ansari, S.A., et al., Nitrogen-doped titanium dioxide (N-doped TiO2) for visible light photocatalysis. New Journal of Chemistry, 2016. 40: p. 3000-3009.

[9] Reszczyńska, J., et al., Visible light activity of rare earth metal doped (Er3+, Yb3+ or Er3+/Yb3+) titania photocatalysts. Applied Catalysis B: Environmental, 2015. 163: p. 40-49.

[10] Reszczyńska, J., et al., Lanthanide co-doped TiO2: The effect of metal type and amount on surface properties and photocatalytic activity. Applied Surface Science, 2014. 307: p. 333-345.

[11] Yang, J., et al., Completely <001> oriented anatase TiO2 nanoarrays: topotactic growth and orientation- related efficient photocatalysis. Nanoscale, 2015. 7(33): p. 13888-13897.

[12] Lamiel-Garcia, O., et al., Adsorption properties of trifluoroacetic acid on anatase (101) and (001) surfaces: a density functional theory study. Phys Chem Chem Phys, 2015. 17(36): p. 23627-23633.

[13] El-Bahy, Z.M., A.A. Ismail and R.M. Mohamed, Enhancement of titania by doping rare earth for photodegradation of organic dye (Direct Blue). Journal of Hazardous Materials, 2009. 166(1): p. 138-143.

[14] Fu, K., et al., Enhanced Photocatalytic Activity of TiO2 Nanorod Arrays Decorated with CdSe Using an Upconversion TiO2:Yb3+, Er3+ Thin Film. Industrial & Engineering Chemistry Research, 2015. 54(2): p. 659-665.

[15] Zhang, Q., et al., Low Ag-Doped Titanium Dioxide Nanosheet Films with Outstanding Antimicrobial Property. Environmental Science & Technology, 2010. 44(21): p. 8270-8275.

[16] Zhang, W., et al., Photocatalytic activity of Ag nanoparticle- dispersed N-TiO2 nanofilms prepared by magnetron sputtering. Environmental Science & Technology, 2010. 5: p. 57155-57163.

[17] Han, X. and G. Shao, Electronic Properties of Rutile TiO2 with Nonmetal Dopants from First Principles. The Journal of Physical Chemistry C, 2011. 115(16): p. 8274-8282.

[18] Panayotov, D.A., et al., Ultraviolet and Visible Photochemistry of Methanol at 3D Mesoporous Networks: TiO2 and Au-TiO2. The Journal of Physical Chemistry C, 2013. 117(29): p. 15035-15049.

[19] Jiang, B., et al., Enhanced Photocatalytic Activity and Electron Transfer Mechanisms of Graphene/TiO2 with Exposed {001} Facets. The Journal of Physical Chemistry C, 2011. 115(48): p. 23718-23725.

[20] Zhang, C., et al., Mesoporous SrF2 and SrF2: Ln3+ (Ln = Ce, Tb, Yb, Er) Hierarchical Microspheres: Hydrothermal Synthesis, Growing Mechanism, and Luminescent Properties. The Journal of Physical Chemistry C, 2010. 114(15): p. 6928-6936.

[21] Zhang, Y., et al., Synthesis of novel yttrium-doped graphene oxide nanocomposite for dye removal. Journal of Materials Chemistry A, 2014. 2(21): p. 7897.

[22] Martins, P.M., et al., Improving Photocatalytic Performance and Recyclability by Development of Er-Doped and Er/Pr-Codoped TiO2/Poly (vinylidene difluoride) - Trifluoroethylene Composite Membranes. The Journal of Physical Chemistry C, 2014. 118(48): p. 27944-27953.

[23] Rodriguez, J.A. and D. Stacchiola, Catalysis and the nature of mixed-metal oxides at the nanometer level: special properties of MOx/TiO2 (110) {M= V, W, Ce} surfaces. Physical Chemistry Chemical Physics, 2010. 12(33): p. 9557.

[24] Wu, Y., et al., Template-free synthesis of mesoporous anatase yttrium-doped TiO2 nanosheet-array films from waste tricolor fluorescent powder with high photocatalytic activity. RSC Advances, 2013. 3(25): p. 9670.

[25] Meksi, M., et al., Design of TiO2 nanorods and nanotubes doped with lanthanum and comparative kinetic study in the photodegradation of formic acid. Catalysis Communications, 2015. 61: p. 107-111.

[26] Rapsomanikis, A., et al., Cerium-modified TiO2 nanocrystalline films for visible light photocatalytic activity. Journal of Photochemistry and Photobiology A: Chemistry, 2014. 280: p. 46-53.

[27] Wang, H., et al., Deactivation mechanism of Ce/TiO2 selective catalytic reduction catalysts by the loading of sodium and calcium salts. Catalysis Science & Technology, 2013. 3(3): p. 715-722.

[28] Duan, Z.G., Z.Y. Zhao and Q.N. Shi, Modification mechanism of praseodymium doping for the photocatalytic performance of TiO2: a combined experimental and theoretical study. Phys Chem Chem Phys, 2015. 17(29): p. 19087-95.

[29] Zhang, H., et al., Anatase TiO2 Crystal Facet Growth: Mechanistic Role of Hydrofluoric Acid and Photoelectrocatalytic Activity. ACS Applied Materials & Interfaces, 2011. 3(7): p. 2472-2478.

[30] Zhang, D., et al., A micrometer-size TiO2 single-crystal photocatalyst with remarkable 80% level of reactive facets. Chemical Communications, 2009(29): p. 4381.

[31] Wang, W., et al., Crystal facet growth behavior and thermal stability of {001} faceted anatase TiO2: mechanistic role of gaseous HF and visible-light photocatalytic activity. CrystEngcomm, 2013. 15: p. 2537–2543.

[32] Ong, W.J., et al., Highly reactive {001} facets of TiO2-based composites: synthesis, formation mechanism and characterization. Nanoscale, 2014. 6(4): p. 1946-2008.

[33] Ye, L., et al., Synthesis of anatase TiO2 nanocrystals with {101}, {001} or {010} single facets of 90% level exposure and liquidphase photocatalytic reduction and oxidation activity orders. J. Mater. Chem. A, 2013. 1: p. 10532–10537.

[34] Xu, J., et al., Unique Anatase TiO2 Twinning Crystals Formed by High-Energy {001} Facets and the Improved Photocatalytic Activity. The Journal of Physical Chemistry C, 2015. 119(23): p. 13011-13020.

[35] Yang, H.G., et al., Anatase TiO2 single crystals with a large percentage of reactive facets. Nature, 2008. 453(7195): p. 638-641.

[36] Liu, B. and E.S. Aydil, Anatase TiO2 films with reactive {001} facets on transparent conductive substrate. Chemical Communications, 2011. 47(33): p. 9507.

[37] Roy, N., Y. Sohn and D. Pradhan, Synergy of Low-Energy {101} and High-Energy {001} TiO2 Crystal Facets for Enhanced Photocatalysis. ACS Nano, 2013. 7(3): p. 2532-2540.

[38] Wang, Y., et al., A selective etching phenomenon on {001} faceted anatase titanium dioxide single crystal surfaces by hydrofluoric acid. Chemical Communications, 2011. 47(10): p. 2829.

[39] Yu, J., et al., Enhanced Photocatalytic CO2-Reduction Activity of Anatase TiO2 by Coexposed {001} and {101} Facets. Journal of the American Chemical Society, 2014. 136(25): p. 8839-8842.

[40] Zhang, Y. and F. Liu, Self-assembly of three shapes of anatase TiO2 nanocrystals into horizontal and vertical two-dimensional superlattices. RSC Advances, 2015. 5: p. 66934-66939.

[41] Harvey, E.J., et al., Characterisation of the (Y1-xLax)2Ti2O7 system by powder diffraction and nuclear magnetic resonance methods. Journal of Materials Chemistry, 2006. 16: p. 4665-4674.

[42] Reszczyńska, J., et al., Photocatalytic activity and luminescence properties of RE3+-TiO2 nanocrystals prepared by sol–gel and hydrothermal methods. Applied Catalysis B: Environmental, 2016. 181: p. 825-837.

[43] Zhao, B., et al., The influence of yttrium dopant on the properties of anatase nanoparticles and the performance of dye-sensitized solar cells. Phys Chem Chem Phys, 2015. 17(22): p. 14836-14842.

[44] Nguyen-Phan, T., et al., The role of rare earth metals in lanthanide-incorporated mesoporous titania. Microporous and Mesoporous Materials, 2009. 119(1-3): p. 290-298.

[45] Luan, Y., et al., Exceptional Photocatalytic Activity of 001-Facet-Exposed TiO2 Mainly Depending on Enhanced Adsorbed Oxygen by Residual Hydrogen Fluoride. ACS Catalysis, 2013. 3(6): p. 1378-1385.

[46] Xu, T., et al., Hydrothermal preparation of nanoporous TiO2 films with exposed {001} facets and superior photocatalytic activity. Journal of Materials Chemistry A, 2015. 3(37): p. 19115-19122.

[47] Yang, H.G., et al., Solvothermal Synthesis and Photoreactivity of Anatase TiO2 Nanosheets with Dominant {001} Facets. Journal of the American Chemical Society, 2009. 131(11): p. 4078-4083.

[48] Sun, L., et al., Study of Homologous Elements: Fe, Co, and Ni Dopant Effects on the Photoreactivity of TiO2 Nanosheets. ChemCatChem, 2014. 6(1): p. 339-347.

[49] Zhang, J., et al., Increasing the Oxygen Vacancy Density on the TiO2 Surface by La-Doping for Dye-Sensitized Solar Cells. J. Phys. Chem. C, 2010. 114(43): p. 18396-18400.

[50] Jampaiah, D., et al., Structural characterization and catalytic evaluation of transition and rare earth metal doped ceria-based solid solutions for elemental mercury oxidation. RSC Advances, 2013. 3(31): p. 12963.

[51] Bouras, K., et al., Insight into photon conversion of Nd3+ doped low temperature grown p and n type tin oxide thin films. RSC Adv., 2016. 6(71): p. 67157-67165.

[52] Qiao, L., et al., The impact of crystal symmetry on the electronic structure and functional properties of complex lanthanum chromium oxides. Journal of Materials Chemistry C, 2013. 1: p. 4527-4535.

[53] Li, G., D. Zhang and J.C. Yu, Thermally stable ordered mesoporous CeO2/TiO2 visible-light photocatalysts. Physical Chemistry Chemical Physics, 2009. 11(19): p. 3775-3782.

[54] Cao, X.P., et al., Synthesis of visible-light responsive C, N and Ce co-doped TiO2 mesoporous membranes via weak alkaline sol-gel process. J. mater. Chem, 2012. 22(30): p. 15309-15315.

[55] Mani, J., et al., Macro-meso-porous TiO2, ZnO and ZnO-TiO2-composite thick films. Properties and application to photocatalysis. Catal. Sci. Technol., 2012. 2(2): p. 379-385.

[56] Sampaio, M.J., et al., Nanodiamond-TiO2 composites for photocatalytic degradation of microcystin-LA in aqueous solutions under simulated solar light. RSC Adv., 2015. 5(72): p. 58363-58370.

[57] Chai, Y., et al., Efficient visible-light photocatalysts from Gd-La codoped TiO2 nanotubes. Ceramics International, 2014. 40(2): p. 2691-2696.

[58] Fang, Y., et al., Systematic Synthesis and Characterization of Single-Crystal Lanthanide Orthophosphate Nanowires. J. AM. CHEM. SOC., 2003. 2003: p. 16025-16034.

[59] Wang, W., et al., Large Ultrathin Anatase TiO2 Nanosheets with Exposed {001} Facets on Graphene for Enhanced Visible Light Photocatalytic Activity. The Journal of Physical Chemistry C, 2012. 116(37): p. 19893-19901.